SEDIMENTOLOGY the journal of the International Association of Sedimentologists

*Sedimentology* (2012) **59,** 1257–1277 doi: 10.1111/j.1365-3091.2011.01305.x

# Meganodular anhydritization: a new mechanism of gypsum to anhydrite conversion (Palaeogene–Neogene, Ebro Basin, North-east Spain)

FEDERICO ORTÍ*, LAURA ROSELL*, ELISABET PLAYÀ* and JOSEP M. SALVANY†
**Departament de Geoquímica, Petrologia i Prospecció Geològica, Universitat de Barcelona (UB), C/Martí i Franqués s/n, 08028 Barcelona, Spain (E-mail: lrosell@ub.edu)*
*†Departament d'Enginyeria del Terreny, Cartogràfica i Geofísica, Universitat Politècnica de Catalunya, C/Gran Capità s/n, 08034 Barcelona, Spain*

Associate Editor – Stephen Lokier

**ABSTRACT**

A number of Palaeogene to Early Neogene gypsum units are located along the southern margins of the Ebro Basin (North-east Spain). These marginal units, of Eocene to Lower Miocene age, formed and accumulated deposits of Ca sulphates (gypsum and anhydrite) in small, shallow saline lakes of low ionic concentration. The lakes were fed mainly by ground water from deep regional aquifers whose recharge areas were located in the mountain chains bounding the basin, and these aquifers recycled and delivered Ca sulphate and Na chloride from Mesozoic evaporites (Triassic and Lower Jurassic). In outcrop, the marginal sulphate units are largely secondary gypsum after anhydrite and exhibit meganodules (from 0·5 to >5 m across) and large irregular masses. In the sub-surface these meganodules and masses are mostly made of anhydrite, which replaced the original primary gypsum. The isotopic composition (11·1 to 17·4‰ for $\delta^{18}O_{VSMOW}$; 10·7 to 15·3‰ for $\delta^{34}S_{VCDT}$) of secondary gypsum in this meganodular facies indicates that the precursor anhydrite derived from *in situ* replacement of an initial primary gypsum. As a result of ascending circulation of deep regional fluid flows through the gypsum units near the basin margins, the gypsum was partly altered to anhydrite within burial conditions from shallow to moderate depths (from some metres to a few hundred metres?). At such depths, the temperatures and solute contents of these regional flows exceeded those of the ground water today. These palaeoflows became anhydritizing solutions and partly altered the subsiding gypsum units before they became totally transformed by deep burial anhydritization. The characteristics of the meganodular anhydritization (for example, size and geometry of the meganodules and irregular masses, spatial arrangement, relations with the associated lithologies and the depositional cycles, presence of an enterolithic vein complex and palaeogeographic distribution) are compared with those of the anhydritization generated both in a sabkha setting or under deep burial conditions, and a number of fundamental differences are highlighted.

**Keywords** Anhydrite, diagenesis, Ebro Basin, evaporites, gypsum, meganodules.

## INTRODUCTION

Anhydrite can grow in a sabkha environment where it forms interstitially in the vadose–capillary fringe and in the upper part of the phreatic zone during very early diagenesis (Curtis *et al.*, 1963; Shearman, 1966; Evans *et al.*, 1969; Butler *et al.*, 1982; Wood *et al.*, 2002; Warren, 2006; Strohmenger *et al.*, 2010). Nevertheless, the most common growth of this mineral in calcium-sulphate evaporite formations occurs in a deep burial setting and results in the total conversion of gypsum to anhydrite. This burial diagenetic process occurs at varying depths, in general >500 m, with increasing values of temperature and lithostatic pressure progressively affecting the subsiding gypsum formations (Murray, 1964; Shearman, 1985). These two modes (sabkha and deep burial) of anhydrite growth have been recognized in many evaporite units in the Palaeogene–Neogene sedimentary basins of Spain both at sub-surface (anhydrite in boreholes and mine galleries) and at the surface. In outcrop, identification of sabkha-type anhydrite has been based on some characteristic facies exhibited by the secondary gypsum rocks, such as nodular, banded-nodular and enterolithic facies, and in deep burial mode by the presence of various facies, including pseudomorphs inherited from the precursor primary gypsum (Ortí, 1989, 1997).

However, a different anhydrite growth mode is recorded in many non-marine evaporite units of the Palaeogene–Neogene Iberian basins. This mode can be characterized by the presence of large (metre-scale) nodules and irregular masses of secondary gypsum in outcrop. A number of authors dealing with these lacustrine units have used the term 'gypsum meganodule' to designate this facies (Ortí, 1989; García Veigas, 1997; Ortí & Rosell, 2007). The anhydrite precursor of this facies has often been attributed to a sabkha setting. In outcrop, this facies of secondary gypsum can coexist with those derived from the hydration of both sabkha and deep burial anhydrite, making genetic discrimination difficult. Gypsum meganodules in the Iberian basins have been traditionally exploited for the high-quality plaster of Paris industry and alabaster sculptures.

The present paper offers new data and a comprehensive interpretation of the meganodular gypsum in the Palaeogene–Neogene Ebro Basin. The main aims of this paper are to establish clear criteria for differentiating this facies from other secondary gypsum facies, and to improve the understanding of its genetic process. This study was only undertaken with gypsum samples obtained from quarry fronts, given that anhydrite samples of this facies at depth were not available.

## GEOLOGICAL AND STRATIGRAPHIC SETTING

The Ebro Basin in NE Spain is a foreland basin that developed during the Palaeogene–Neogene. Bounding mountain chains in the south of the basin are the Iberian Chain in the south-west and the Catalan Coastal Range in the south-east, both of which consist of Palaeozoic and Mesozoic rocks. In the Iberian Chain, the last contractional phases occurred during the Miocene when the materials of the chain overthrusted the Palaeogene basinal sediments. In the Catalan Coastal Range, contraction structures (WNW-verging folds and thrusts) occurred during the Palaeogene and were controlled by pre-existing basement faults (Guimerà & Álvaro, 1990; Casas, 1992).

The southern margin of the Ebro Basin is defined by the Iberian and Catalan margins. These two margins involve the respective contact zones between the Mesozoic and Palaeozoic materials (Fig. 1) of the bounding mountain chains and the sediments of the Palaeogene–Neogene basin fill. In the Iberian margin, the Lower Miocene deposits onlap the Palaeogene units. In the Catalan margin of the basin, the Palaeogene deposits range in age from Early Eocene to Early Oligocene (Fig. 1A).

A number of non-marine evaporite units are recorded in the Ebro Basin. These units were formed in two types of saline lakes (Fig. 2) (Ortí *et al.*, 1989a,b). In the first case, Type A, there were small saline lakes near the southern margins of the basin characterized by waters with low ionic concentration and a Ca-sulphate composition. The units that accumulated in these lakes, i.e. 'marginal gypsum units' (Fig. 1A and B), have a thickness of <100 m. The most frequent deposit in these units, i.e. 'Type A gypsum facies', is a microcrystalline bioturbated gypsum, which is a shallow-water product common in other Palaeogene–Neogene Iberian basins (Rodríguez-Aranda & Calvo, 1998; Ortí *et al.*, 2003). Locally, clastic gypsum (mainly gypsarenites) accompany the bioturbated gypsum facies, together with nodular secondary gypsum derived from the hydration of anhydrite nodules formed in a sabkha setting developed around the saline lakes. In addition to gypsum, small amounts of carbonate, lutite and chert are present in these marginal units.

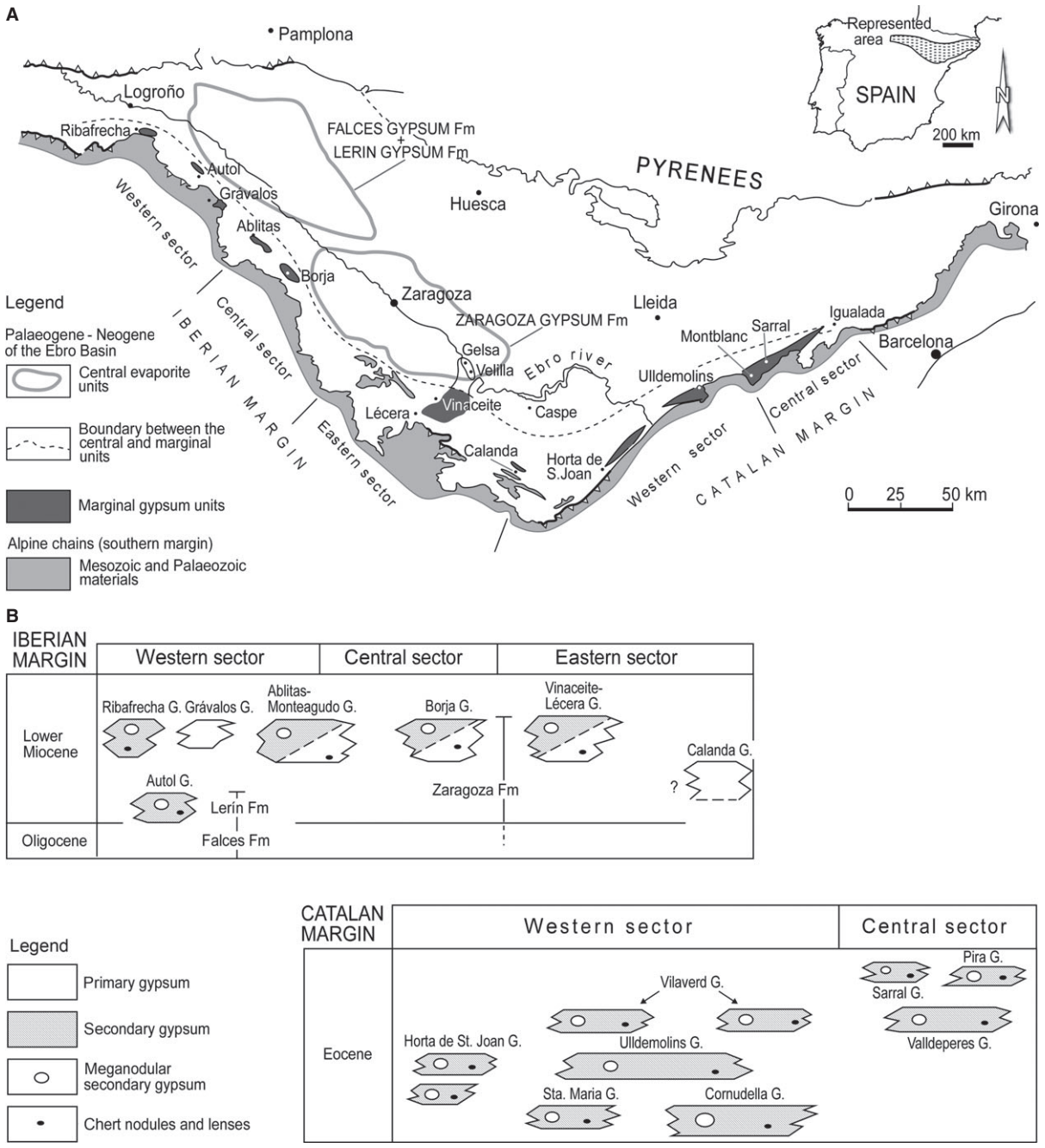


**Fig. 1.** Palaeogene to Early Neogene lacustrine evaporite units in the Iberian and Catalan margins of the Ebro Basin. Structural sectors (western, central and eastern) are distinguished in these margins. (A) Geographical location of the marginal gypsum units. Additionally, the distribution of some central evaporite units (Falces Gypsum Formation, Lerín Gypsum Formation and Zaragoza Gypsum Formation) is shown (other central evaporite units of both lacustrine and marine origins are omitted in this figure). Mesozoic materials: lutites, sandstones, carbonates and evaporites. Palaeozoic materials: slates, schists, graywackes, sandstones, conglomerates, carbonates and igneous rocks. (B) Stratigraphic position of the marginal gypsum units. Units in the Iberian margin: Autol Gypsum, Grávalos Gypsum, Ablitas-Monteagudo Gypsum, Borja Gypsum, Lécera-Vinaceite Gypsum and Calanda Gypsum. Units in the Catalan margin: Horta de Sant Joan Gypsum, Sta. Maria del Montsant Gypsum, Ulldemolins Gypsum, Cornudella Gypsum, Vilaverd Gypsum, Valldeperes Gypsum, Pira Gypsum and Sarral Gypsum. The most significant evaporite facies in these units are indicated. In the Iberian margin, the stratigraphic position (vertical lines) of the central evaporite units is shown. In this margin, the Ablitas-Monteagudo Gypsum and the Borja Gypsum units were connected laterally with the Zaragoza Gypsum Formation, while the Grávalos Gypsum and the Ribafrecha Gypsum units were not connected with any central evaporite unit. Adapted from Ortí (1997, figs, 8.3 and 8.4).

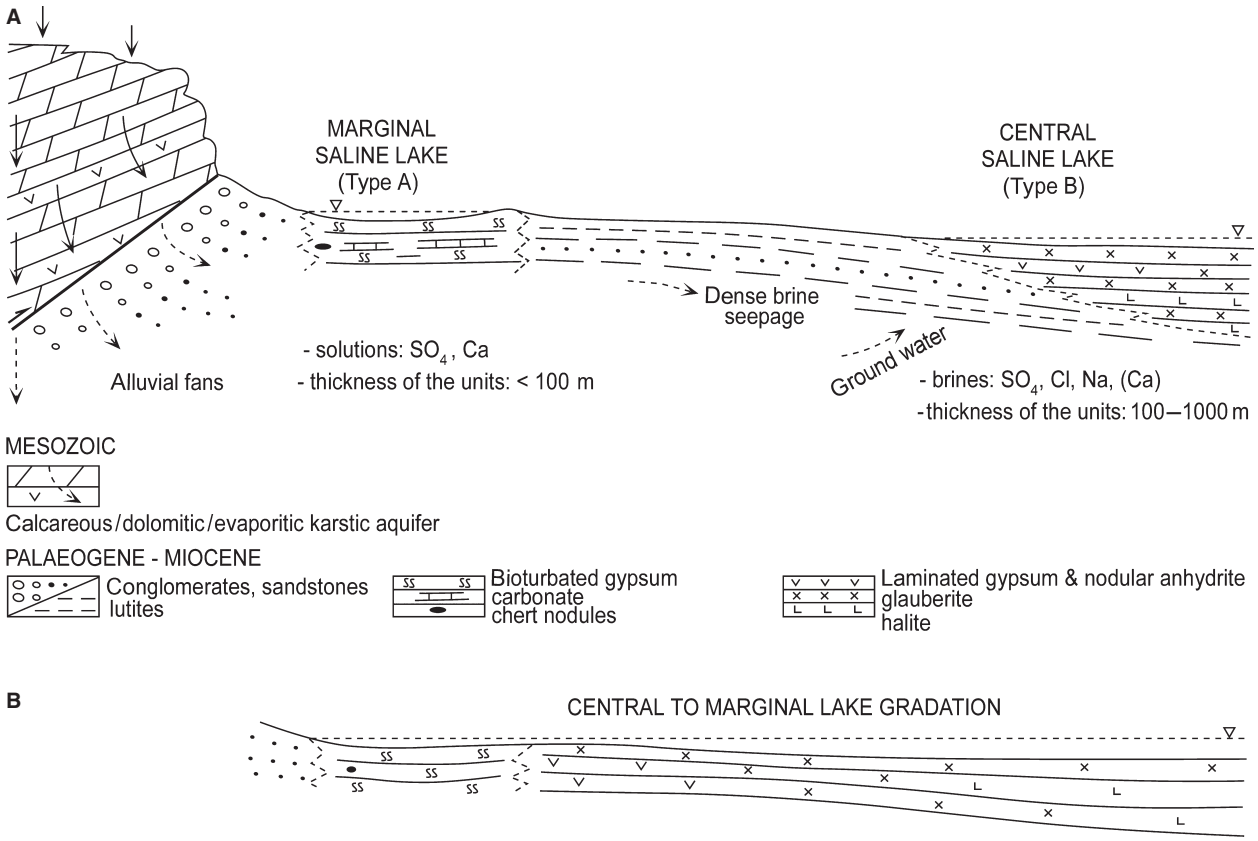


**Fig. 2.** Saline lake types and associated facies in the Palaeogene to Early Neogene evaporites of the Ebro Basin. Interpretative scheme out of scale. (A) General case in which the marginal gypsum units are not connected with the central evaporite units. (B) Case in which a marginal gypsum unit changes laterally to a central evaporite unit.

Included in the second case, Type B, were large saline lakes located towards the centre of the basin characterized by waters with high ionic concentration and a Na-sulphate or Na-chloride composition. The units accumulated in these lakes, i.e. 'central evaporite units' (Fig. 1A), have an individual thickness of several hundred metres. The most common facies in these units, i.e. 'Type B gypsum facies', is an alternation of laminated gypsum and bedded-nodular gypsum. At the surface, this facies is commonly formed by secondary gypsum. At the subsurface, it changes to anhydrite in association with halite and glauberite beds (Salvany & Ortí, 1994; Salvany *et al.*, 2007). Some of these central evaporite units grade laterally to the marginal gypsum units (Fig. 2B) or may develop a ring of Type A gypsum facies locally.

The marginal gypsum units and the central evaporite units accumulated in shallow lakes. Sulphate in the mother waters of all these lakes was derived from chemical recycling of Mesozoic (Triassic and Lower Jurassic) marine evaporites present in the bounding mountain chains and the basin substratum (Utrilla *et al.*, 1991, 1992).

## Marginal gypsum units

The evaporite sediments cropping out in the Iberian margin of the Ebro Basin include gypsum units that were deposited during two major episodes of the Early Miocene (Salvany *et al.*, 1994) (Fig. 1B). During the first episode of Agenian age (a non-marine mammal stage equivalent to Aquitanian), the Autol Gypsum formed. This unit was coeval with the central evaporites of the Lerín Gypsum Formation (Fig. 1A) and graded laterally into it. During the second episode of Aragonian age (equivalent to Burdigalian), a number of marginal units accumulated coevally with the central evaporites of the Zaragoza Gypsum Formation (Fig. 1 A). Some of these marginal units were connected laterally to the basin-centre evaporites of the Zaragoza Gypsum Formation while others were separated from them. All these marginal units grade laterally into siliciclastic formations. The Zaragoza Gypsum Formation developed a gypsum ring in its south-western zone.

The Palaeogene sediments cropping out in the Catalan margin include small gypsum units interbedded with lutites, sandstones and con-

glomerates, and fresh water limestones and marls (Fig. 1B). These marginal units accumulated from the Ilerdian (Lower Eocene) to the Priabonian (Upper Eocene) (Fig. 1B). The presence of evaporite cycles is a common feature in these units. Due to the absence of sub-surface data it is not possible to precisely constrain lateral variations in evaporite facies between marginal and central units. One case has been documented in which a central evaporite unit (Clariana Gypsum unit; Ortí *et al.*, 2007) displays a ring of Type A gypsum facies close to the Catalan margin.

Occurrences of meganodules (Fig. 3A and B) and large irregular masses of secondary gypsum are recorded in many of the marginal gypsum units along both the Iberian and Catalan margins of the Ebro Basin (Ortí, 1997), as well as in the gypsum rings of some central evaporite units. Hereafter these occurrences and associated features will be termed 'meganodular facies' and the

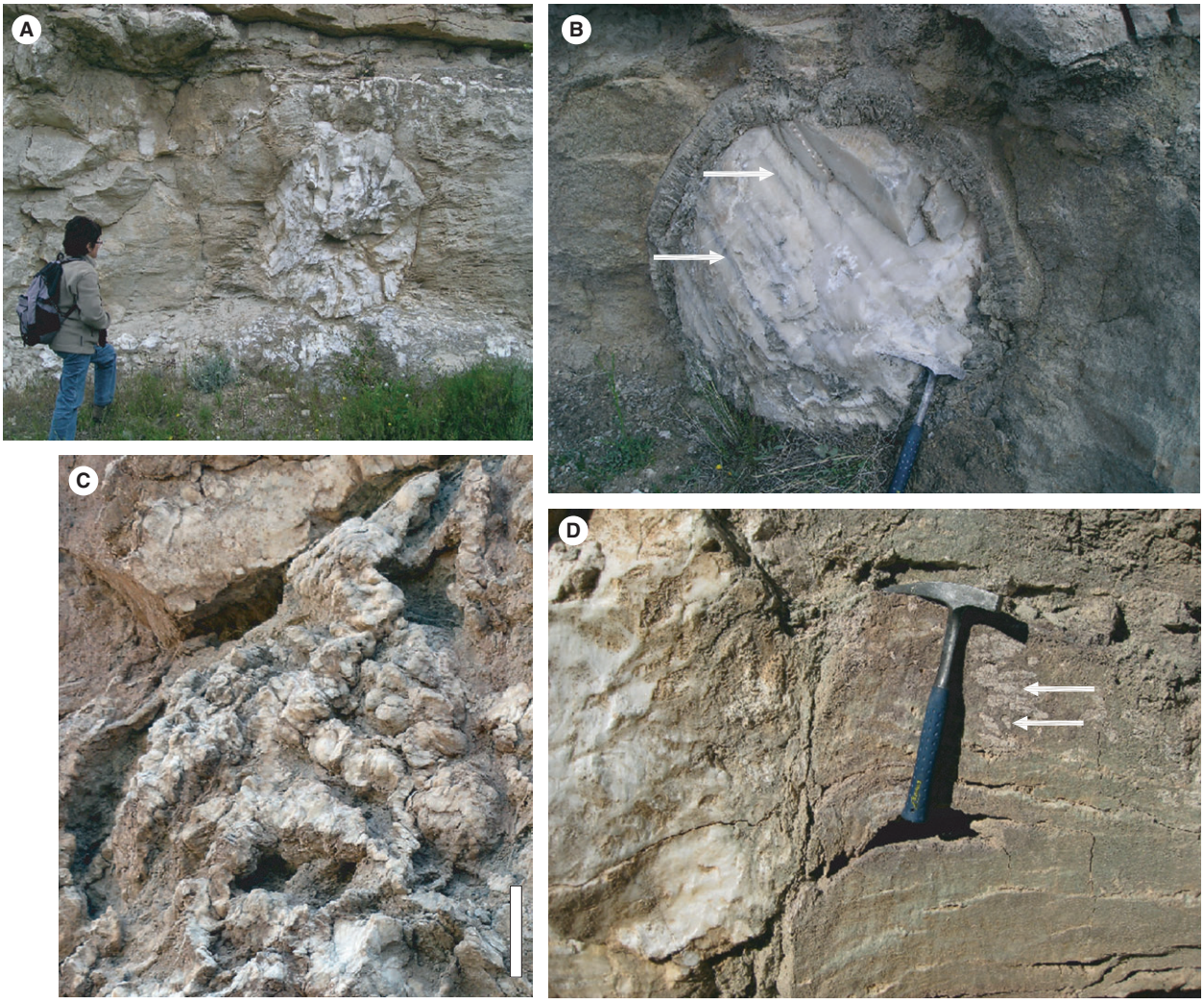


**Fig. 3.** Meganodular facies: some particular aspects. (A) Isolated meganodule of alabastrine secondary gypsum. Host-rock is also secondary gypsum, which derived from a precursor facies of primary, bioturbated gypsum. Note the replacive character of the meganodule on the gypsum host-rock. Person for scale is *ca* 1·6 m tall. (B) Isolated meganodule formed by megacrystalline secondary gypsum. Host-rock is primary gypsum. Note the replacive character of the meganodule on the gypsum host-rock as well as the uniformity of the cleavage plains (dark lines; arrows) indicating that only one megacrystal forms the meganodule. Hammer for scale is 32 cm long. (C) Detail of an enterolithic vein complex. This complex is formed by alabastrine secondary gypsum veins surrounding a gypsum meganodule (not visible in the picture). The veins are oriented in different directions within a lutite host-rock. Bar: 20 cm. (D) Contact between a meganodule made up of alabastrine secondary gypsum and its host-rock formed by secondary gypsum. This host-rock bears burrows filled by micritic carbonate (arrows). Note the total destruction of burrows within the meganodule.

 

process generating this facies will be termed 'meganodular anhydritization'.

## MATERIALS AND METHODS

All of the known occurrences of meganodular facies in the marginal gypsum units of the Ebro Basin were visited. Representative pairs of gypsum samples were taken in many of these occurrences. In these pairs, one sample corresponds to the secondary gypsum in the meganodular facies and the other to the gypsum (primary or secondary) of the host-rock, the two samples being located adjacent to each other on both sides of the contact between the meganodule and the host-rock. About 50 of these pairs of samples were selected for mineralogical control (X-ray diffraction) and for petrographic study in thin section (5·5 × 5·4 cm). The isotopic composition ($\delta^{18}O_{VSMOW}$ and $\delta^{34}S_{VCDT}$ of $SO_4$) was determined in 12 of these pairs of gypsum samples.

The isotope determinations were carried out in: (i) the Servicio de Isótopos Estables of the Universidad de Salamanca following the methods of Longinelli & Craig (1967) for oxygen and of Robinson & Kusakabe (1975) for sulphur. Reproducibility was within the range of ±0·27‰ for sulphur and ±0·07‰ for oxygen; and (ii) in the Serveis Cientificotècnics (Laboratori d'Isòtops Estables) of the Universitat de Barcelona where, after dissolving gypsum and precipitating $BaSO_4$, the analyses were conducted using a Mass Spectrometer (IRMS), Delta Plus XP Finnigan (Thermo Fisher Scientific, Madison, WI, USA); for the $\delta^{34}S$ isotope determinations the spectrometer was connected to an elemental analyser system (EA), Carlo Erba 1108; for the $\delta^{18}O$ isotope determinations the spectrometer was connected to a pyrolysis device TC/EA, Thermo Fisher.

Analytical error ($2\sigma$) tested by the laboratory was about ±0·40‰ for both determinations. All the values are reported versus VCDT (Vienna Canyon Diablo Troilite) for $\delta^{34}S$ and versus VSMOW (Vienna Standard Mean Ocean Water) for $\delta^{18}O$.

## RESULTS

### Petrology

The mineralogy of the evaporite samples is basically made up of gypsum, anhydrite and celestite as sulphates, calcite and dolomite as carbonates, and some quartz. The petrographic study sought to distinguish between the primary or secondary character of the gypsum textures. The terminology of secondary gypsum used in this paper differentiates between alabastrine (fine-grained crystals, in general <100 μm in size), porphyroblastic (coarser crystals up to 2 cm in size) and megacrystalline (very large crystals, from >2 cm up to 1 m) textures. The primary gypsum of the bioturbated facies is formed by microlenticular crystals, in general <1 mm across, totally devoid of anhydrite inclusions. In the samples made up of secondary gypsum, the most common texture is alabastrine, but porphyroblastic textures are also observed, mainly forming external coatings on the meganodules; exceptionally, the meganodules are totally or partly made up of megacrystalline textures (Fig. 3B). Tiny inclusions of precursor anhydrite crystals (relics) are always present in the porphyroblastic and megacrystalline textures and, to a lesser extent, in the alabastrine textures. Small crystals of celestite usually accompany the primary and secondary gypsum textures. Carbonates with micritic textures are associated with the meganodular facies and the gypsum host-rock. Quartz (as chert nodules) is mainly composed of the length-slow varieties of authigenic chalcedony (lutecite and quartzine).

### Occurrences

In the Iberian margin of the Ebro Basin, the meganodular facies is absent in the Grávalos Gypsum and the Calanda Gypsum, but it is well-developed in the rest of the gypsum units (Fig. 1A). In the units bearing meganodules (Fig. 1B), the gypsum host-rock is formed by primary gypsum, which is the most common case, or by secondary gypsum, which is the case of the Autol Gypsum (this old unit underwent deep burial and the bioturbated primary gypsum was totally transformed into anhydrite). In these units, meganodules and large irregular masses of secondary gypsum, ranging between 50 cm and 3 m across, form discontinuous layers parallel to the stratification or display sub-vertical arrangement cross-cutting the bedding. The meganodular facies replaces and/or displaces the gypsum host-rock and is also overprinted on other host lithologies (lutites, carbonates and chert nodules). For instance, in the Ablitas-Monteagudo Gypsum unit, the meganodules appear both in the primary bioturbated gypsum and in the nodular secondary gypsum (Salvany *et al.*, 1994; Ortí & Salvany, 1997). Moreover, the meganodular facies occurs in

the zone between the villages of Velilla and Gelsa, where a gypsum ring of the Zaragoza Gypsum Formation is present. Examples of meganodular occurrences are shown in Fig. 4 (Ribafrecha Gypsum) and Fig. 5 (Gelsa-Velilla gypsum rim).

In the marginal units of the Catalan margin, gypsum is always secondary in outcrop given that all these units were deeply buried and the bioturbated gypsum underwent burial anhydritization (Ortí, 1997; Ortí *et al.*, 2007). In these units, the meganodules and irregular masses of secondary gypsum have diameters and lengths reaching several metres across, and their distribution oscillates from sub-parallel to sub-vertical to bedding. This meganodular facies replaces/displaces any pre-existing gypsum facies and may deform the bedding. The meganodules and irregular masses can be surrounded by a complex of enterolithic gypsum veins oriented in all directions (Fig. 3C); they can also be surrounded by patches of the lutite host-rock, displaying severe deformation. The gypsum host-rock in all these units is always secondary.

The Sarral Gypsum unit in the central sector of the Catalan margin is representative of the gypsum units along this margin (Fig. 1B). The meganodular facies of this unit in the quarries near the village of Sarral is shown in Fig. 6A and a scheme of the spatial distribution of the irregular masses and meganodules is shown in Fig. 6B. In the Sarral Gypsum unit, the evaporite cycles consist of three depositional intervals (Fig. 6B): (i) the base consists of red and grey gypsiferous lutites; (ii) the intermediate interval is an alternation of gypsiferous red lutites and gypsum beds in which the meganodular facies is moderately developed; and (iii) the upper interval consists of thick (2 to 10 m) gypsum beds bearing chert and carbonate, in which the meganodular facies is extensively developed. Some pedogenetic features and vestiges of dissolution are common at the top of this upper interval.

## Characterization of the meganodular facies

In the assemblage of the marginal gypsum units of the Ebro Basin, the meganodular facies can be characterized using a number of features, such as size and geometry, spatial arrangement, relationships with the associated lithologies, presence of enterolithic vein complex, relationships with the depositional cycles and palaeogeographic distribution. The size of the meganodular features is very variable. Individualized meganodules can attain a diameter of 5 m, but the irregular masses can occupy significant portions of the quarry fronts with lengths over 20 m across. The shape of the meganodules is also very variable, ranging from almost spherical to polygonal or irregular. Meganodules can be single or composite, and their internal structures grade from massive to multinodular, although textural zoning (concentric banding) is systematically absent. Locally, elongated, cylinder-like masses appear in the outer zone of the meganodules projecting against the host-rocks (Fig. 5B). The boundaries between the meganodules grade from almost planar to concave–convex or to sutured, and the contacts between the meganodules and the irregular masses oscillate from sharp to gradual. Deformation structures in the meganodules and irregular masses are common, including a flow-like appearance.

The most frequent arrangement of the meganodular facies is stratiform, but a sub-vertical arrangement is often observed (Figs 4 and 6). In the latter case, columns or walls up to 5 to 6 m in height are observed locally.

Some features should be recorded in the host lithologies of the meganodular facies. The gypsum host-rock can be replaced or displaced. Bedding deformation can be a common feature including flow-like, residual patches of lutite beds surrounding the meganodules or trapped within them. Chert nodules enclosed within the meganodules can be broken locally into separate pieces. The host-carbonate can be wholly displaced/replaced by meganodular facies (Fig. 3D). A complex of enterolithic veins of secondary gypsum oriented in all directions is commonly enclosed within the gypsum host-rock, as well as within the patches of lutite surrounding the meganodules (Fig. 3C). When cycles are present in the gypsum units, the meganodular facies is predominantly developed in the thick (2 to 10 m) gypsum beds forming the upper intervals (Fig. 6B). In contrast, this facies is rare or absent in the cycles that display thinner (<2 m) gypsum beds in these intervals.

The meganodular facies is present discontinuously in the gypsum units along the basin margins. It occurs in positions close to these margins in the gypsum rings of the central evaporite units.

## Isotopes

The isotopic composition of sulphate ($\delta^{34}S_{VCDT}$, $\delta^{18}O_{VSMOW}$) in gypsum samples was obtained in the marginal units of the Iberian and Catalan margins. Moreover, some determinations were made in samples of the gypsiferous rings of the central evaporite units. All these analyses corre-

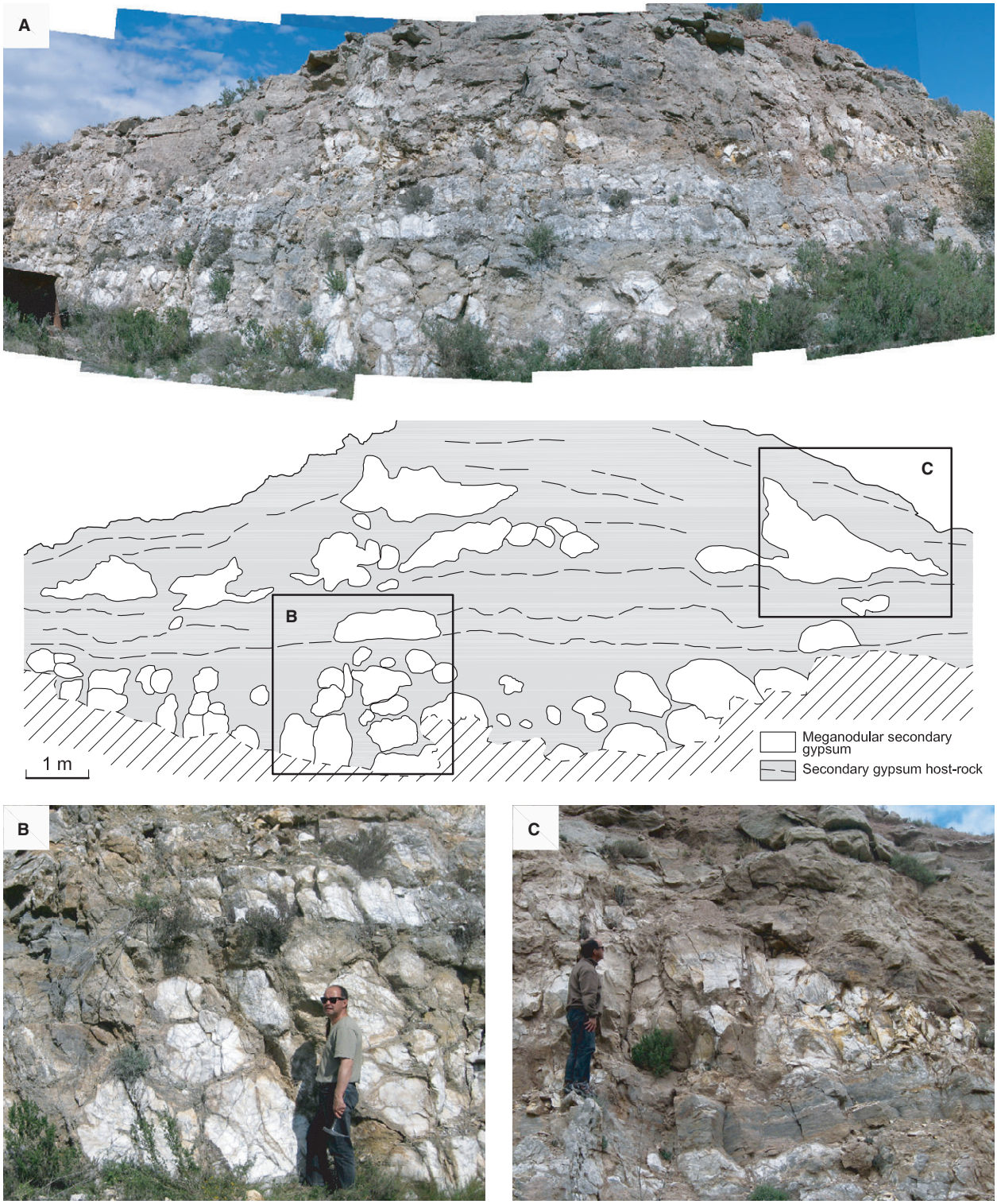


**Fig. 4.** Meganodular facies in the Iberian margin of the Ebro Basin. Ribafrecha Gypsum unit (Lower Miocene; La Rioja). Quarry to the north-west of the Ribafrecha village. (A) Panoramic view and scheme of a portion of the quarry front. (B) and (C) Pictures of sub-vertical and stratiform arrangements of the secondary gypsum meganodules and irregular masses. The host-rock is also made up of secondary gypsum. Persons for scale are *ca* 1·7 m tall.

spond to 12 pairs of samples from the meganodules and their adjacent gypsum host-rocks. The results show values ranging from 11·1 to 17·4‰ for $\delta^{18}O_{VSMOW}$ and from 10·7 to 15·3 $\delta$‰ for $^{34}S_{VCDT}$ (Table 1 and Fig. 7). Each pair of samples also show similar values for both $\delta^{18}O$ and $\delta^{34}S$

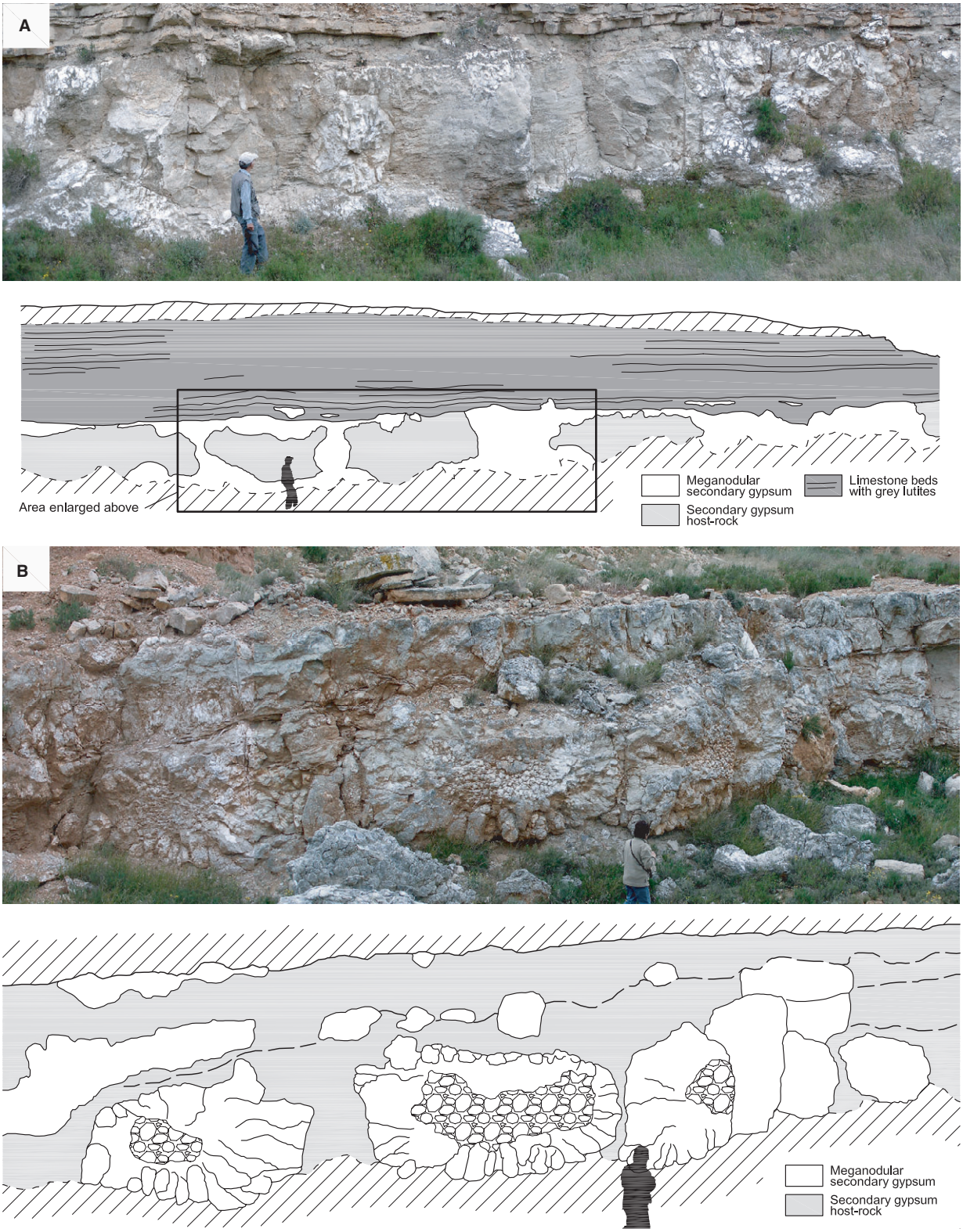


**Fig. 5.** Meganodular facies in the gypsum ring of the Zaragoza Gypsum Formation (Lower Miocene). Gelsa-Velilla area in the quarries to the north of the Velilla village (Zaragoza province, Iberian margin of the Ebro Basin). Note persons for scale *ca* 1·7 m tall. (A) Panoramic view and scheme of a portion of the quarry front. Note the sub-vertical arrangement of the meganodules and irregular masses (white colour). (B) Panoramic view and scheme of another portion of the same quarry front. Note the stratiform arrangement of the meganodules, as well as their multinodular cores and their radially oriented, elongated outer zones.

 

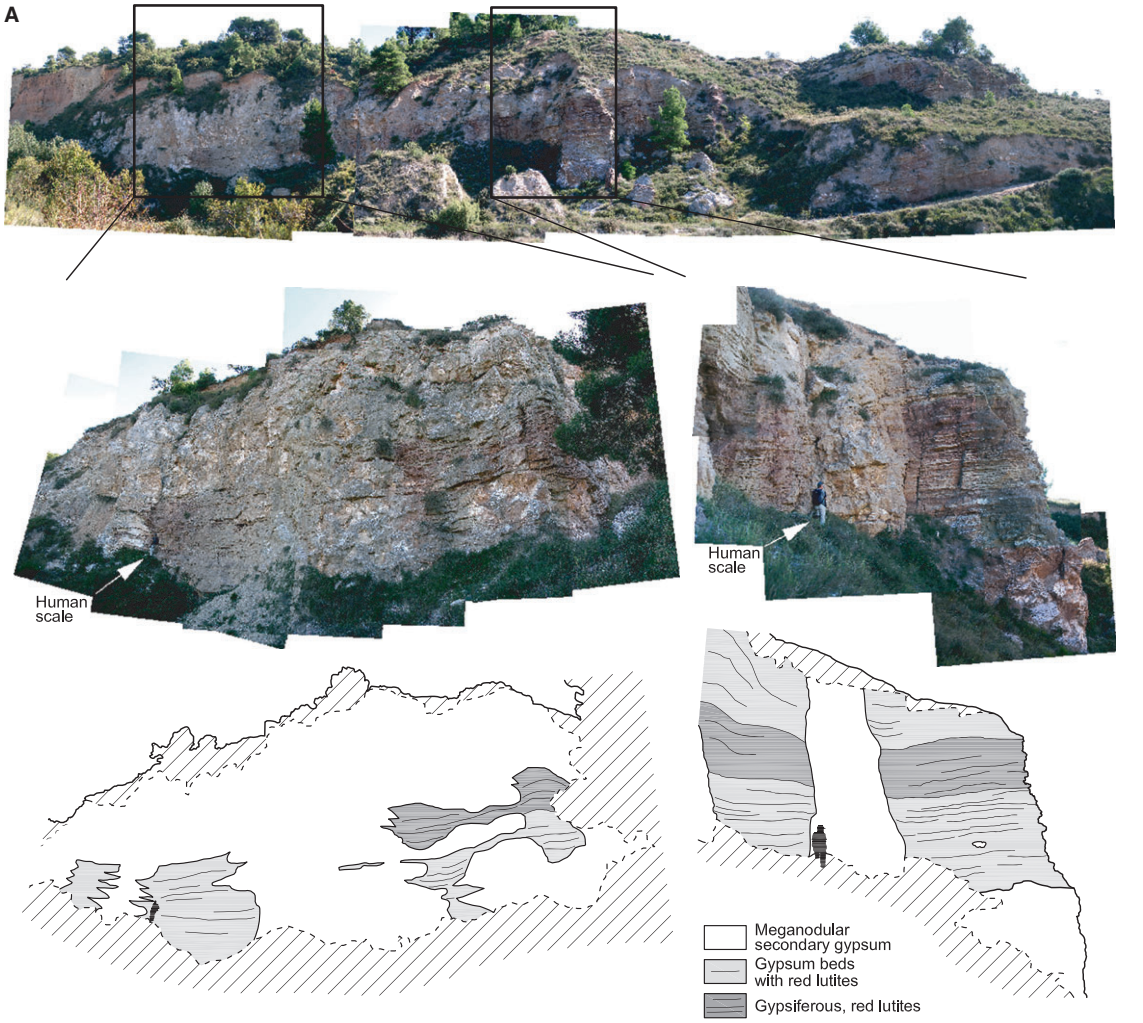
A
Human scale
Human scale
Meganodular secondary gypsum
Gypsum beds with red lutites
Gypsiferous, red lutites
B
Stratigraphic intervals
Occurrence of meganodular facies
Cycles
B3
B2
A3
B
A
3
2
3
2
1
10 m
5 m
10 m
Legend:
Quarry front
Sedimentary cycle
Secondary gypsum
Clay, marl
Chert
Meganodules and irregular masses of gypsum
Enterolithic veins of gypsum
Clay, marl remains within the gypsum
Gypsum micronodules and small pseudomorphs

**Fig. 6.** Meganodular facies in the Catalan margin of the Ebro Basin: the Sarral Gypsum unit (Tarragona province; Upper Eocene), in the quarry near the 'Roman' dam, about 800 m to the west of the Sarral village. (A) Upper picture: general view of the quarry front. Lower pictures and associated schemes: on the left, the stratiform arrangement of the meganodules is predominant; on the right, the vertical arrangement is shown. Note persons for scale *ca* 1·7 m tall. (B) General scheme of the distribution of meganodules and irregular masses of secondary gypsum in this quarry front. On the left part of the figure, two depositional cycles ('A' and 'B') and their intervals ('1' to '3') are indicated. In the column of the stratigraphic intervals (A3 to B3), the original undisturbed bedding is interpreted; on the right, the stratiform and vertical arrangements of the meganodular facies are shown. The meganodular anhydritization totally affects the upper intervals of the cycles (A3 and B3) and partly the intermediate interval (B2).

with only minor variations ranging from −0·5 to +0·76‰ for $\delta^{18}O_{VSMOW}$ and from −0·5 to +0·5‰ for $\delta^{34}S_{VCDT}$.

## DISCUSSION

### Isotope interpretation

The $\delta^{34}S$ and $\delta^{18}O$ values in the pairs of selected samples show that no significant differences exist between the two samples of each pair regardless of the current nature (primary or secondary) of the host gypsum (Fig. 7). These values also confirm the former interpretation that a chemical recycling from Triassic sulphates (8·9 to 14·9‰ for $\delta^{18}O_{VSMOW}$; 10·2 to 16·6 $\delta$‰ for $^{34}S_{VCDT}$; Utrilla *et al.*, 1991) occurred in the Palaeogene–Neogene Ebro Basin (Utrilla *et al.*, 1992). However, the $\delta^{18}O$ values are slightly heavier than those of the Triassic range, suggesting that redox processes linked to sulphate-reducing bacterial activity

**Table 1.** Isotopic values ($\delta^{18}O_{VSMOW}$, $\delta^{34}S_{VCDT}$, in ‰) of pairs of gypsum samples in the gypsum units of the southern margins of the Palaeogene–Neogene Ebro Basin. All values are positive. The units are indicated in Fig. 1B. Samples Vel-22 correspond to the gypsum ring of the Zaragoza Gypsum Formation in the area between Gelsa and Velilla villages. Samples RQ-1 correspond to the Rocafort Gypsum unit (marked with an asterisk), which is a small unit overlying the Sarral Gypsum unit not represented in Fig. 1B.

| Margin (age of the units) | Stratigraphic unit | Pairs of samples and facies | | Gypsum type | $\delta^{18}O_{VSMOW}$ (‰) | $\delta^{34}S_{VCDT}$ (‰) |
|---|---|---|---|---|---|---|
| Iberian (Miocene) | Ribafrecha Gypsum | VB-22a | Meganodule | Secondary | 14.2 | 14.5 |
| | | VB-22b | Massive host gypsum | Secondary | 14.3 | 14.7 |
| | Velilla-Gelsa gypsum ring | Vel-22a | Meganodule | Secondary | 15.6 | 14.3 |
| | | Vel-22b | Massive host gypsum | Secondary | 15.3 | 14.2 |
| | Autol Gypsum | AV-21a | Meganodule | Secondary | 11.4 | 10.8 |
| | | AV-21b | Massive host gypsum | Secondary | 11.1 | 10.7 |
| | Ablitas-Monteagudo Gypsum | ABL-22a | Meganodule | Secondary | 13.9 | 13.4 |
| | | ABL-22b | Massive host gypsum | Primary | 13.3 | 13.1 |
| | | ABL-20a | Meganodule | Secondary | 13.3 | 13.0 |
| | | ABL-20b | Massive host gypsum | Primary | 13.1 | 13.2 |
| Catalan (Eocene) | Rocafort Gypsum* | RQ-1a | Meganodule | Secondary | 13.8 | 14.5 |
| | | RQ-1b | Massive host gypsum | Secondary | 13.1 | 14.3 |
| | Sarral Gypsum | Sa-1a' | Meganodule | Secondary | 15.1 | 13.9 |
| | | Sa-1b' | Massive host gypsum | Secondary | 14.3 | 14.4 |
| | Pira Gypsum | Ol-4a | Meganodule | Secondary | 15.2 | 15.0 |
| | | Ol-4b | Massive host gypsum | Secondary | 14.8 | 15.1 |
| | | Pi-1a | Meganodule | Secondary | 16.6 | 14.4 |
| | | Pi-1b | Massive host gypsum | Secondary | 17.0 | 14.5 |
| | | Pi-2Aa | Meganodule | Secondary | 16.7 | 15.3 |
| | | Pi-2Ab | Massive host gypsum | Secondary | 16.1 | 14.8 |
| | | Pi-3a | Meganodule | Secondary | 16.1 | 15.3 |
| | | Pi-3b | Massive host gypsum | Secondary | 16.2 | 15.2 |
| | Vilaverd Gypsum | VI-1a | Meganodule | Secondary | 16.9 | 13.6 |
| | | VI-1b | Massive host gypsum | Secondary | 17.4 | 13.2 |

 

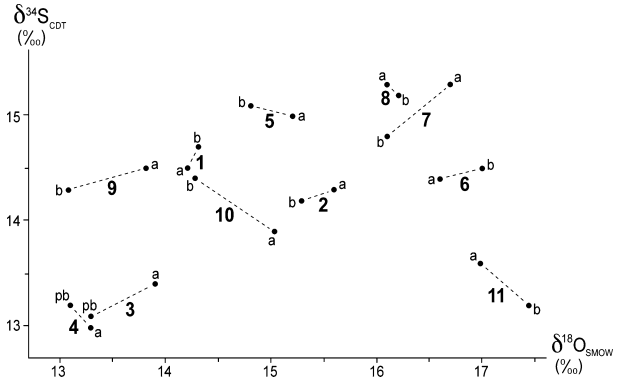


**Fig. 7.** Isotopic values ($\delta^{34}S_{VCDT}$ versus $\delta^{18}O_{VSMOW}$, in ‰) of pairs of gypsum samples: 'a' alabastrine secondary gypsum of the meganodules; 'b' secondary gypsum host-rock (derived from bioturbated gypsum); 'pb' bioturbated gypsum host-rock preserved as primary. The correspondence with pairs of samples in Table 1 is as follows: 1: VB-22; 2: Vel-22; 3: Abl-22; 4: Abl-20; 5: Ol-4; 6: Pi-1; 7: Pi-2A; 8: Pi-3; 9: RQ-1; 10: Sa-1. 11: Vi-1. The pair AV-21 (Table 1) with values very different from the rest of the pairs is not included in this figure.

occurred in the saline lakes (Pierre, 1982, 1985; Utrilla *et al.*, 1991).

Given that the isotope composition of sulphate does not undergo a change in the anhydrite conversion to secondary gypsum (Worden *et al.*, 1997), the $\delta^{34}S$ values suggest that the precursor meganodular anhydrite mainly formed from the *in situ* replacement of the primary gypsum of the marginal lakes. Assuming that some sulphate was supplied by the anhydritizing fluids, the isotope composition would be practically the same as the primary gypsum and the Triassic sulphates.

## Criteria against sabkha or deep burial interpretations

The characteristics of the meganodular facies are clearly different from those derived from a deep burial diagenesis or a sabkha setting. As regards the deep burial origin, one factor should be borne in mind. The growth of the meganodules is not related to deep burial diagenesis because they coexist with unaffected primary gypsum facies in several Miocene units of the Iberian margin (Fig. 1B).

As for the sabkha setting, the following factors seem to contradict this possible origin: (i) the abnormally large size of the anhydritized bodies; (ii) the systematic lack of erosion/dissolution surfaces at the top of the meganodules; (iii) the large-scale deformation that this facies may exert on bedding and other sedimentary structures; (iv) the common arrangement of this facies in sub-vertical walls or columns; (v) the overprinting of meganodules on gypsum facies which formed coevally and graded laterally into each other (Salvany *et al.*, 1994; fig. 12); (vi) the difference in geometry between the enterolithic vein complex, in random orientation, and the interbedded enterolithic levels of a sabkha deposit; (vii) the effect this facies has on other lithologies such as carbonate displacement/replacement or the breakage of chert nodules; and (viii) the lack of evidence for microbial facies (Lokier & Steuber, 2008).

In the case of the aforementioned gypsum cycles bearing meganodular facies (Fig. 6B), which are present in the central sector of the Catalan margin, the following interpretation has been proposed (Ortí *et al.*, 2007): (i) microlenticular bioturbated gypsum was the original facies in all the intervals of the cycle; (ii) meganodules and irregular masses of anhydrite formed within the gypsum layers of the intermediate and upper intervals after the accumulation of the whole cycle; and (iii) the rest of the bioturbated gypsum became anhydritized by deep burial diagenesis. Thus, the distribution of the meganodules in the cycles mainly reflects their selective growth within the thickest gypsum beds. Ortí *et al.* (2007) assumed a shallow to moderate burial (tens of metres?) origin for this mode of anhydrite growth.

The vertical arrangement of the meganodular facies could also suggest a growth linked to the presence of huge (metre-scale) desiccation cracks that formed during subaerial episodes in a manner similar to those in some halite formations (Marchal, 1983; Lugli, 1999; Lugli *et al.*, 1999). However, the following observations seem to challenge such an interpretation for this facies in the Ebro Basin: (i) the absence of vertical fractures in the gypsum host-rock; (ii) the absence of any type of fracture-filling matrix associated with the sub-vertical meganodules; and (iii) the fact that the base of the columns often exceeds the top in width. The vertical arrangement could also suggest the presence of late karstic features. However, neither cavities nor any type of karst-filling material were recognized in association with the meganodules.

## Other meganodular occurrences

Recently the existence of secondary gypsum meganodules in a number of Palaeogene–Neogene basins in the Iberain domain has been

documented in Ortí *et al.* (2010), particularly in the Calatayud, Tremp and Tajo (Madrid) basins, in the Coastal Depression of València, and in some other localities. Many features in these occurrences are similar to those described in the present paper for the case of the Ebro Basin: the large size of the meganodules, reaching up to 8 m in diameter locally; their vertical arrangement in walls or columns in some cases, as in the Calatayud Basin where they reach up to 20 m in height and several metres in width (Ortí & Rosell, 2000); the presence of Triassic and Lower Jurassic evaporites in the mountain chains bounding the basins; and the palaeogeographic position close to the basin margins. Ortí *et al.* (2010) assigned the meganodular occurrences in these Iberian basins to the alteration of gypsum by the ascending circulation of fluids under burial conditions.

In contrast to the Iberian occurrences, scarce examples of gypsum or anhydrite meganodules in other geological domains are available. The presence of secondary gypsum meganodules in a vertical arrangement in the Mazan Gypsum unit (South-east France), of Palaeogene age, has been cited and attributed to the action of highly saline ascending flows (Truc, 1983; Ortí *et al.*, 2010). In a Messinian evaporite section in the Volterra Basin from western Tuscani (Castellina Marittima, Pisa, Italy), the presence of secondary gypsum 'alabaster spheroids' up to 1·5 m in diameter was cited by Lugli & Testa (1993). These spheroids developed as anhydrite within clastic layers of selenitic gypsum. Lugli & Testa (1993) concluded that: ''sabkhatization and dissolution of former halite layers may account for irregular massive anhydritization of autochthonous selenite and development of displacive anhydrite spheroids within the clastic gypsum layers''. In the Neogene Iskenderun Basin in the south of Turkey, the presence of 'gypsum/anhydrite balls' with diameters up to 1·5 cm is known, although a clear explanation for this occurrence, which constitutes one of the facies of the Messinian evaporites in the basin, is not yet available.

In a completely different setting, the presence of anhydrite facies bearing nodules with diameters ranging between a few millimetres up to several metres has been cited in the Miocene Kuroko deposits of the Hokuroko Basin (north-eastern Japan) in association with strata-bound sulphide ores (Shikazono *et al.*, 1983). Primary fluid inclusions in the anhydrite reveal temperatures of the fluids between 240°C and 340°C. This anhydrite, as well as other sulphates (gypsum and barite) present in these deposits, has been attributed to hydrothermal convection systems (Kuroda, 1977).

## Gypsum to anhydrite conversion by burial: factors and fluid types

Primary gypsum converts to anhydrite by burial at variable depths depending on the basin conditions. Some of the factors controlling this conversion are temperature, salinity of the interstitial fluids and balance between lithostatic and hydrostatic pressures (Warren, 2006). Temperature is the most important factor in cases such as in the geothermal field of Salton Sea (USA) where the conversion occurs at a depth of <200 to 250 m and at a temperature of 80 to 105°C (Osborn, 1989).

The interaction between salinity and temperature in the stability fields of gypsum and anhydrite has been studied by many authors. Calculations by MacDonald (1953) showed that gypsum is the stable phase below 40 to 42°C in water saturated only with Ca and $SO_4$, and that anhydrite is the stable phase above this temperature, despite the fact that the transition temperature would be significantly lowered by the addition of NaCl. Other authors agree that the high salinity of the solution (or low activity of the water, $\alpha_{H2O}$) contributes to a significant decrease in the temperature of the gypsum to anhydrite transition (Bock, 1961; Marshall & Slusher, 1966; Hardie, 1967). In some Holocene coastal sabkhas dominated by halite-saturated pore-fluids, the conversion occurs interstitially at depths of only 1 m or less and at a temperature of 35 to 40°C (Kinsman, 1969, 1976). In the case of ancient chloride-rich basins, where the gypsum sediments were in contact with highly saline pore waters, a gypsum to anhydrite transformation could occur from synsedimentary conditions to shallow to moderate burial depths, for example, in the Badenian Carpathian Foredeep in Poland (Kasprzyk & Ortí, 1998; Kasprzyk, 2003).

The ratio between lithostatic and hydrostatic pressures is influenced by the permeability of the host-rock, which also plays a role in the gypsum to anhydrite conversion. During this conversion, the crystallization water of the gypsum is lost and a decrease of about 39% in the volume of the solid phase can be achieved. If the host-rock allows free drainage, the lithostatic pressure of the overburden is taken up in the solid phase, facilitating the conversion at shallower burial depths. If water cannot escape freely, it becomes geopressured and also takes up the lithostatic

 

pressure inducing the complete transformation at greater depths (Hanshaw & Bredehoeft, 1968; Jowett *et al.*, 1993; Testa & Lugli, 2000).

In addition to these factors, the type of solutions circulating through the evaporites at depth should be considered in the gypsum to anhydrite conversion. The ionic composition of many basinal waters indicates mixtures in varying proportions between at least three types of fluids: original brines trapped interstitially in the evaporite units, compaction waters from adjacent evaporite units and head-driven, deeply circulating (regional aquifers) meteoric inflows (Moldovanyi & Walter, 1992; Land, 1995a,b).

In ancient formations bearing interstitial brines, the temperature at which the gypsum to anhydrite conversion occurred can be estimated by the lithologies associated with the Ca-sulphate units. According to Hovorka (1992) and Warren (2006), when common siliciclastic (shales and sandstones) or carbonate units accompany the sulphates, this temperature could be about 50°C, corresponding to depths of 450 to 500 m under normal geothermal gradients (Murray, 1964). When the sulphate beds show evidence of coeval halite or early diagenetic halite cement, the temperature could descend to 20°C and the conversion would occur at shallower depths (Hardie, 1967).

Compaction of evaporite units bearing very soluble minerals can generate large volumes of highly saline pore brines. The lateral and vertical circulation of such brines can affect the adjacent and the overlying gypsum units. Bäuerle *et al.* (2000) estimated a gypsum to anhydrite conversion depth of only 125 m in the Hauptanhydrite under the influence of ascending compaction fluids from the underlying Zechstein 2 Salt.

The two former types of solutions only consider the pore fluids originally present in the evaporite units. However, the head-driven, deeply meteoric flows circulating at depth through the basin sediments (regional aquifers) also cause mineral reactions in the evaporite units. These flows should also be taken into account, in particular when their ionic concentration and/or temperature are relatively high.

## Palaeohydrology of the southern margins of the Ebro Basin

The present hydrological system in the margins of this basin may be used as a guide to deduce the palaeohydrological system during the Palaeogene to Early Neogene (Miocene). The best-known present day system is that of the Iberian margin, which may be summed up by a number of studies (Martínez-Gil *et al.*, 1988; San Román *et al.*, 1989; Sánchez Navarro *et al.*, 1992, 2004; Coloma López *et al.*, 1997; Sánchez *et al.*, 1999). According to these authors, the ground water discharge of the Iberian Chain in the basin currently occurs mainly through the 'Lower Liassic karstic aquifer', i.e. the aquifer at the base of the Lower Jurassic, which is made up of dolostones, limestones and Ca-sulphate beds, the last lithology including a gypsum-anhydrite unit over 300 m thick (Bordonaba & Aurell, 2002; Ortí & Salvany, 2004). Two types of discharge are derived from this aquifer at present; in local springs and diffusely in wetlands. In the former discharge type (Table 2; Fig. 8A), notable springs occur along the contact zone between the Iberian Chain and the basin sediments. The main features of these springs are the following: constant flow rate; high mineralization averaging 1 to 2 g $l^{-1}$; marked Ca-sulphate composition with minor concentrations of $HCO_3^-$, $Cl^-$, $Na^+$, $Mg^{2+}$ and Si (although a high content up to 7 g $l^{-1}$ in NaCl is recorded locally); constant and relatively high temperatures (up to 23 to 24°C), as well as high geothermal gradients in the discharge zones; and low or null tritium content. These characteristics correspond to ground water from deep regional flows with a long-term residence period. Some springs located in the western sector of the margin, such as the Fitero and Arnedillo springs, are thermal and highly mineralized (46°C and 50°C, and 4·5 g $l^{-1}$ and 7·5 g $l^{-1}$, respectively) and have a markedly elevated NaCl composition (Table 2). All of these springs are related to tectonic structures, which induce ground water to move upwards through the basinal sediments and to flow out as springs in a position controlled by the thrust fronts or the anticline axes (Coloma López *et al.*, 1997) (Fig. 8B). Moreover, a number of boreholes reaching the Lower Liassic aquifer near the zone of the mountain chain–basin contact record water temperatures >30°C, as in the Belchite (32°C) and the Aguilón (40°C) boreholes. In many boreholes drilled towards the basin centre, the salinity of the water exceeds 2 g $l^{-1}$ (Sánchez Navarro *et al.*, 2004).

Sánchez *et al.* (1999) suggested that the hydrological system of the Iberian margin during the Palaeogene to Early Neogene was relatively similar to that of today (Fig. 8B). According to these authors, under the closed-basin conditions at that time, the ground water discharge mainly occurred diffusely in the basin centre, creating large saline

**Table 2.** Main parameters of some springs related to regional ground water flows from the Iberian Chain into the present-day Ebro Basin. Springs: 1: Arnedillo; 2: Fitero; 3: San Juan; 4: Borja; 5: Santa Ana y Heras; 6: Pontiel y Toroñel; 7: Virgen de Muel; 8: Virgen de Magdalena; 9: La Cultia; 10: Virgen de Arcos; 11: Los Fontales; 12: Font Calent. Symbols: h a.s.l.: height above sea level; Q: discharge; RS: solid residuum: T: temperature. The location of these springs is indicated in Fig. 8A. Simplified from Sánchez *et al.* (1999; Table 1).

| Springs | h. a.s.l. (m) | Q (L $sec^{-1}$) | RS (mg $l^{-1}$) | T (ºC) | $HCO_3^-$ (meq $l^{-1}$) | $SO_4^{2-}$ (meq $l^{-1}$) | $Cl^-$ (meq $l^{-1}$) | $Ca^{2+}$ (meq $l^{-1}$) | $Mg^{2+}$ (meq $l^{-1}$) | $Na^+$ (meq $l^{-1}$) | $K^+$ (meq $l^{-1}$) |
|---|---|---|---|---|---|---|---|---|---|---|---|
| 1 | 710 | 20 | 6728 | 52.5 | 2.9 | 31.4 | 98.5 | 22.5 | 5.8 | 103.5 | 0.7 |
| 2 | 490 | 50 | 4689 | 46.0 | 2.9 | 27.9 | 44.8 | 24.7 | 8.1 | 43.9 | 0.7 |
| 3 | 490 | 200 | 492 | 18.0 | 3.4 | 3.5 | 1.4 | 5.2 | 1.6 | 1.8 | 0.1 |
| 4 | 450 | 500 | 806 | 18.0 | 3.0 | 3.7 | 2.7 | 5.0 | 2.0 | 2.6 | 0.0 |
| 5 | 430 | 40 | 3426 | 20.0 | 5.0 | 39.0 | 7.7 | 34.0 | 8.0 | 10.9 | 0.2 |
| 6 | 290 | 500 | 1024 | 23.0 | 3.6 | 10.6 | 2.2 | 10.4 | 3.0 | 2.3 | 0.1 |
| 7 | 400 | 100 | 776 | 18.0 | 5.4 | 3.7 | 1.2 | 7.2 | 2.2 | 1.1 | 0.1 |
| 8 | 310 | 200 | 1100 | 23.0 | 3.9 | 8.4 | 5.6 | 7.2 | 4.8 | 6.5 | 0.1 |
| 9 | 355 | 50 | 2700 | 18.0 | 2.8 | 37.5 | 4.5 | 20.6 | 21.6 | 5.8 | 0.4 |
| 10 | 440 | 800 | 2406 | 22.0 | 3.4 | 25.9 | 2.6 | 26.0 | 4.4 | 2.7 | 0.1 |
| 11 | 570 | 1000 | 1130 | 18.0 | 3.5 | 9.7 | 0.3 | 10.2 | 3.6 | 0.3 | 0.1 |
| 12 | 430 | 150 | 623 | 22.0 | 4.5 | 6.0 | 0.3 | 7.2 | 3.2 | 0.1 | 0.1 |

lakes precipitating highly soluble mineral parageneses. The discharge, however, also occurred in the basin margin, giving rise to small saline lakes where low solubility minerals were formed. These lakes were fed by ground water flows through the thick Palaeogene to Early Neogene alluvial deposits. These flows, however, discharged diffusely and did not give rise to localized springs as they do at present, but rather to marginal wetlands in which saline lakes developed (Sánchez *et al.*, 1999). Field observations (previously described in the *Geological and stratigraphic setting* section) also indicate that some inner sabkhas developed in association with these marginal lakes.

Presumably, a similar palaeohydrological system operated in the south-eastern margin of the basin where the Catalan Coastal Range was formed coevally with the accumulation of many marginal gypsum units and some central evaporite ones (Fig. 1B). The Pliocene, however, experienced a progressive change in basin drainage. At present, this margin drains into the Mediterranean Sea and cannot be used for comparative purposes.

## Diagenetic model of meganodular anhydritization

Some of the foregoing ideas were considered by Salvany *et al.* (1994) to account for the gypsum precipitation in the small saline lakes of the Iberian margin during the Miocene. To explain the meganodular anhydritization, the present paper uses a model that takes into account the diagenetic evolution of these gypsum deposits during burial (Fig. 9). The model assumes that during shallow to moderate burial (from some metres to a few hundred metres?) the ascending meteoric flows crossed the subsiding gypsum units causing their partial anhydritization. It is possible that the following factors facilitated the mineral conversion under these burial conditions. Firstly, the temperature of the ascending flows was probably higher (>25°C, on average) than at present; this is because the levels from which the flows ascended were deeper during the Miocene when, in contrast to the present situation, the thick Palaeogene to Early Neogene deposits were not eroded by any fluvial network, as suggested by Coloma López *et al.* (1997) and Sánchez *et al.* (1999). Secondly, the ascending flows presumably had higher salinities than at present. In fact, large volumes of Triassic salt were remobilized and dissolved during the Palaeogene to Early Neogene phases of tectonism and diapirism. In the Iberian margin of the basin, a large proportion of these chlorides was leached by the 'Lower Liassic aquifer'. At present, high NaCl contents are only recorded in the thermal springs of Arnedillo and Fitero (Table 2) whose waters ascend vertically from a depth of 2000 to 2500 m after dissolving residual masses of Triassic salt (Sánchez *et al.*, 1999). Thirdly, highly saline pore-brines that were expelled from the central evaporite units by progressive compaction presumably circulated through the adjacent, marginal gypsum units. These waters probably mixed with the head-driven, deeply ascending and

 

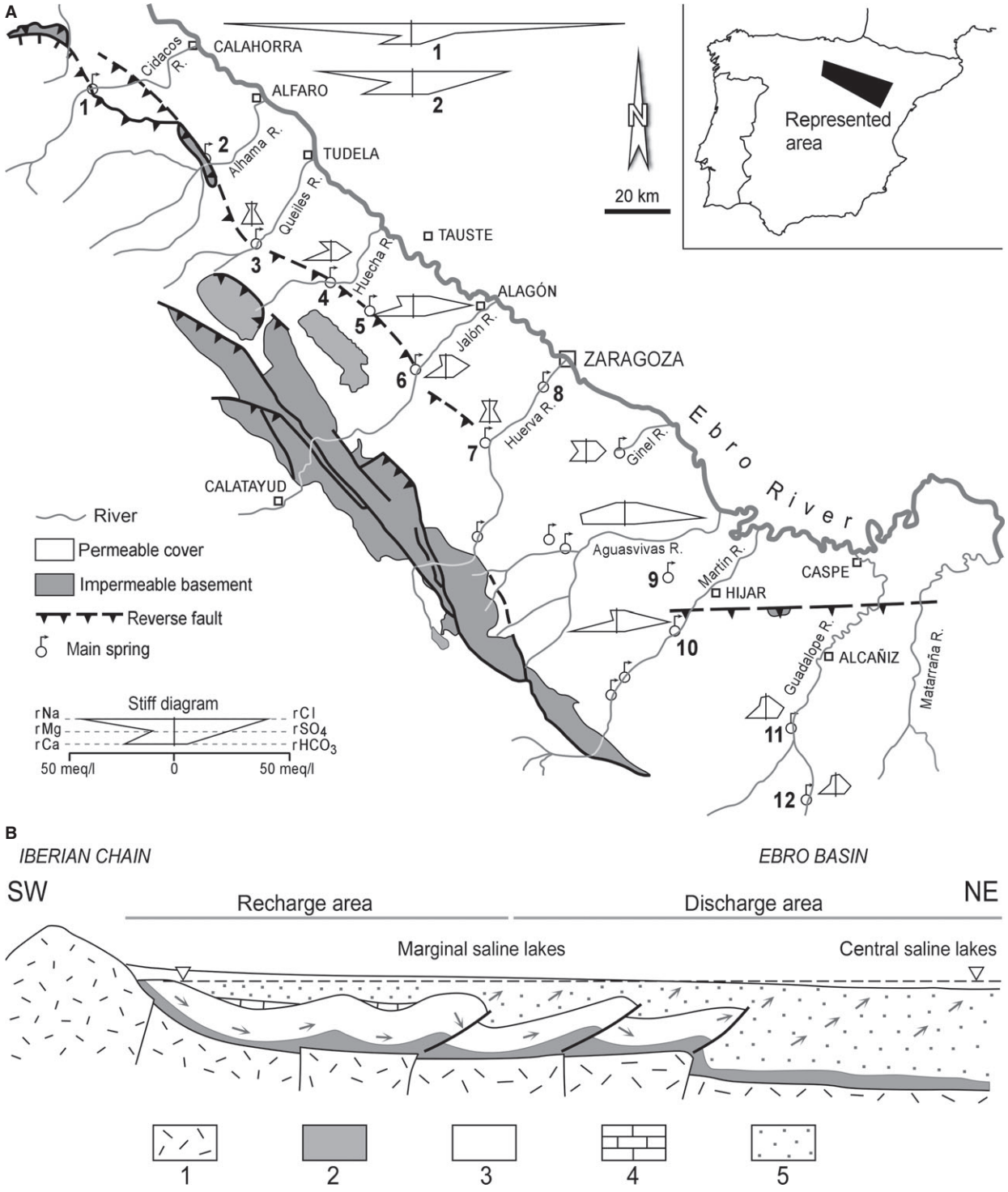


**Fig. 8.** Some aspects of the hydrological and palaeohydrological discharges of the Iberian Chain to the Ebro Basin. (A) Current distribution of some of the major springs along the contact zone between the mountain chain and the basin. Stiff diagrams of the springs are included. Springs as in Table 2. Simplified from Sánchez *et al.* (1999; fig. 4). (B) Reconstructed geological cross-section normal to the basin margin at the end of the Miocene (before partial erosion of the basin-fill), in which the palaeohydrological discharge is illustrated. Lithologies: 1: Palaeozoic and Lower Triassic; 2: Triassic (Muschelkalk and Keuper facies); 3: Early Jurassic to Cretaceous (Aptian); 4: Cretaceous (Albian) to Late Cretaceous; 5: Cenozoic (Late Eocene to Late Miocene). Lithology 1 roughly corresponds to the 'impermeable basement' in (A). Scheme, out of scale, slightly modified from Sánchez *et al.* (1999; fig. 5).

 

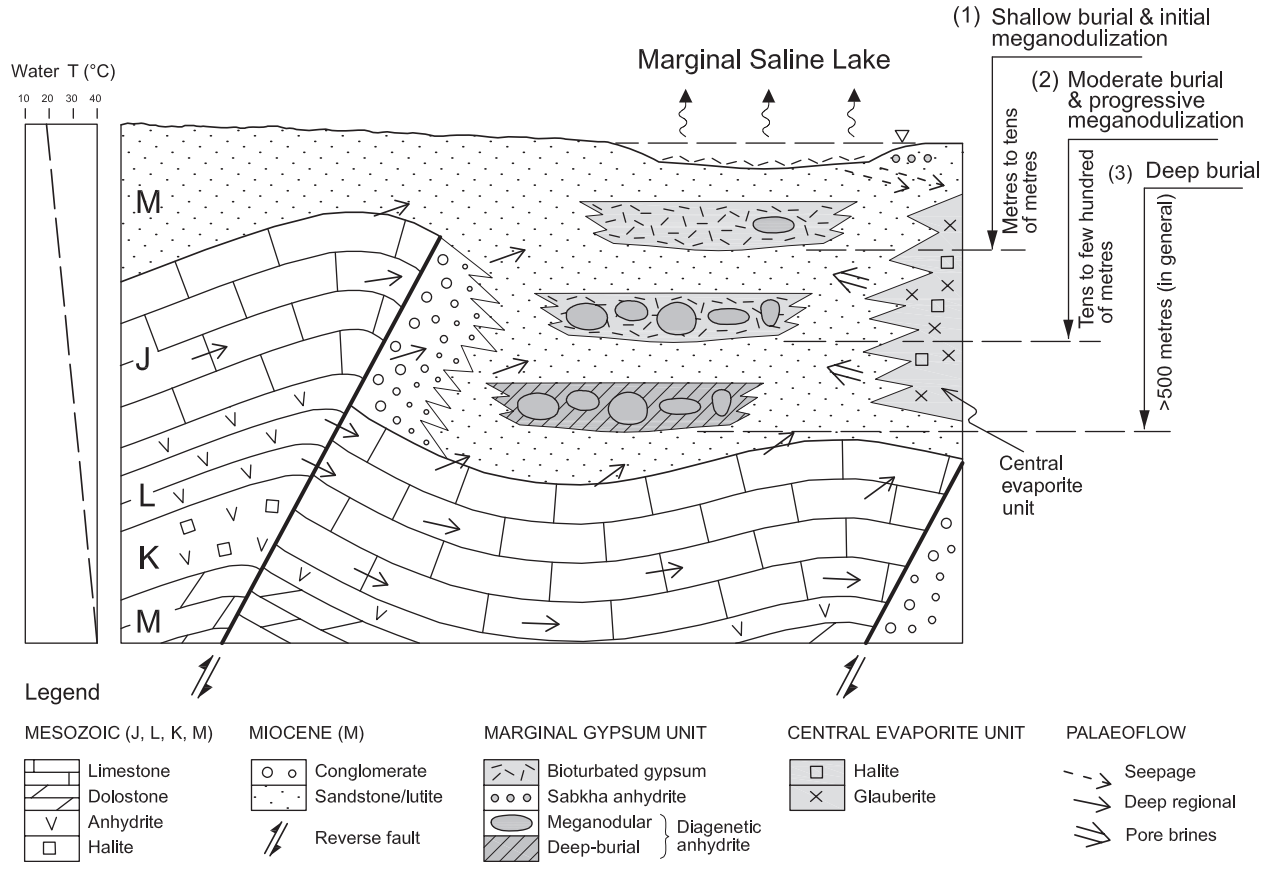


**Fig. 9.** Interpretative model of meganodular anhydritization in the marginal gypsum units of the Ebro Basin during the Miocene. The process (growth of displacive/replacive meganodules and irregular masses of anhydrite) occurs progressively during shallow to moderate burial (Stages 1 and 2). Under deeper burial conditions the preserved primary gypsum hosting the anhydritized portions is also converted to anhydrite (Stage 3). The anticline structures roughly correspond to those represented in the central part of Fig. 8B. 'M' Muschelkalk facies (Middle Triassic); 'K' Keuper facies (Upper Triassic); 'L' Lower Jurassic (Lower Liassic); 'J' Jurassic; 'M' Miocene.

already mineralized (meteoric) ground water. Mixing resulted in a salinity increase in the ground water and facilitated the gypsum to anhydrite conversion at shallower depths. Fourthly, the compositional water released from the gypsum dehydration probably escaped through the adjacent detrital rocks (alluvial fan shales, sandstones and conglomerates; Salvany *et al.*, 1994; Muñoz-Jiménez, 1992) avoiding hydraulic overpressure and facilitating the mineral conversion.

In summary, a double effect, sedimentological and diagenetic, could have derived from the deep flows in the marginal gypsum units of the Ebro Basin during the Palaeogene to Early Neogene. During sedimentation, surface discharge of these flows generated small lakes in which water was concentrated by evaporation, resulting in the precipitation of primary gypsum facies. Seepage reflux of the denser, interstitial solutions from these lakes towards the basin centre prevented the precipitation of halite in the lakes. Some sabkha anhydrite also formed locally. During burial, the envisaged stages of diagenetic evolution of these deposits would be as follows (Fig. 9). Firstly, part of the primary gypsum in these units underwent a meganodular anhydritization during shallow burial. Secondly, progressive meganodulization occurred during moderate burial maintaining contact at depth with the warmer and mineralized ascending flows. Thirdly, in the oldest units, the unaffected portions of primary gypsum underwent total anhydritization when the units were deeply buried (>500 m, in general). Finally, the various genetic types of anhydrite (sabkha, meganodular and deep burial) were rehydrated into secondary gypsum during final exhumation of all the units. A possible origin of this meganodulization because of very hot (hydrothermal) fluids seems to be unlikely given

that no evidence was found in support of: (i) mineralization of ore deposits other than sulphates; (ii) presence of calcareous or siliceous travertines; and (iii) presence of minerals that characterize metaevaporites (Moine *et al.*, 1981).

The model (Fig. 9) presented here can account for the strict similarity of the isotopic values ($\delta^{34}S$ and $\delta^{18}O$) of the meganodular facies to those of the gypsum host-rock. It therefore seems reasonable to assume that only the sulphate of the gypsum available in the marginal units was consumed in the growth of meganodular anhydrite. This possibility is reinforced by the fact that the meganodules and irregular masses are limited to the gypsum units and are lacking in the underlying or overlying units.

This diagenetic model is also in agreement with two observations: (i) the meganodular anhydritization inhomogeneously affected the subsiding gypsum units; and (ii) it was limited in space and time (not all the units along the two basin margins were affected). It seems very likely that the process was controlled by local factors, such as tectonic structures, higher temperature and/or higher salinity of the regional ground water, or preferential circulation pathways of highly saline compaction waters.

The geometry of the meganodules suggests slow and continuous growth of the anhydrite, resulting in a large size and the absence of textural zoning. Such growth seems to be consistent with the circulation of regional flows, also slow and continuous, allowing long-term contacts between the ascending fluids and the subsiding gypsum units.

The common flow-like appearance of meganodules and irregular masses could have been controlled by at least two factors: the incompletely lithified character of the gypsum at the time of its conversion to anhydrite and the considerable loss of volume involved in this process. The combination of these factors could have induced differential compaction between the unaffected portions of the gypsum units and the masses that were anhydritized. This differentiation would have facilitated the presence of flow, mechanical redistribution, deformation and fluid overpressure in these units. Additionally, these conditions probably resulted in the formation of enterolithic veins of anhydrite, which surrounded the meganodules. Warren (1991) argued that a dewatering gypsum bed can convert into a quicksand-like consistency should the released water not drain freely, which results in thick sequences of enterolithic folds with crestal fold vergences oriented in the minimum stress direction.

## CONCLUSION

The textural characteristics of the secondary gypsum rocks making up the meganodular facies in the gypsum units of the southern margins of the Palaeogene–Neogene Ebro Basin confirm that this facies originated as anhydrite. The isotopic compositions ($\delta^{34}S$ and $\delta^{18}O$) of the secondary gypsum in this facies are very similar to those of the gypsum host-rocks, whether primary or secondary gypsum, suggesting that the precursor anhydrite growth mainly occurred by *in situ* replacement of the gypsum forming these units.

The large size of the meganodular features that originated in this process, together with the fact that they are devoid of textural zoning, suggest that the anhydrite growth was slow and continuous, which is consistent with the circulation of deep regional aquifers acting as anhydritizing flows. This process affected the subsiding, marginal gypsum units prior to their complete lithification.

The meganodular anhydritization was basically controlled at depth by the same palaeohydraulic systems that fed the marginal saline lakes at the surface. During the progressive burial of the marginal gypsum units, the mineral change and associated meganodulization occurred in contact with the ascending fluids in which temperature and salinity exceeded (>25°C; richer in Na-chloride) those in the regional hydraulic systems of today. Presumably, this anhydritization occurred during shallow to moderate burial (from metres to few hundred metres). There is no evidence to suggest that supplies of very hot (hydrothermal) flows caused the meganodular anhydritization.

The characteristics of this anhydritization mode clearly differ from those in the sabkha setting. Moreover, these characteristics bear no relation to those derived from deep burial diagenesis, which brought about a total gypsum to anhydrite conversion of the deposits.

It is thought that processes similar to the meganodular anhydritization could also have occurred in other ancient evaporite basins similar to the Ebro Basin. In this scenario, observations of meganodular facies in the evaporite units of these basins would suggest the proximity to a palaeogeographic basin margin or the presence of a palaeohydrological system involving recycling of older evaporites or both.

## ACKNOWLEDGEMENTS

This study was supported by projects CGL2009-11096 of the Spanish Government (*Ministerio de Ciencia e Innovación*) and 2009SGR1451 of the Catalan Government (*Departament d'Innovació, Universitats i Empresa*). The authors thank Dr. J.A. Sánchez Navarro (*Universidad de Zaragoza)* for supplying literature on the hydrological and palaeohydrological systems of the Ebro Basin, Dr. F.J. García-Veigas (*Universitat de Barcelona*) for constructive comments on the chemistry of the palaeofluids and Dr. E. Turkmen (*Ankara University*) for personal communication about evaporite facies in Neogene basins in Turkey (May 2008). The authors are indebted to reviewers B. Charlotte Schreiber and Stefano Lugli and Editors Stephen Lokier and Peter Swart for helpful comments that improved the manuscript.

## REFERENCES

**Bäuerle, G., Bornemann, O., Mauthe, F.** and **Michalzik, D.** (2000) Origin of stylolites in Upper Permian Zechstein Anhydrite (Gorleben Salt Dome, Germany). *J. Sed. Res.*, **70,** 726–737.

**Bock, E.** (1961) On the solubility of anhydrous calcium sulfate and of gypsum in concentrated solutions of sodium chloride at 25°C, 30°C, and 50°C. *Can. J. Chem.*, **39,** 1746–1751.

**Bordonaba, A.P.** and **Aurell, M.** (2002) Variación lateral de facies en el Jurásico basal de la Cordillera Ibérica Central: origen diagenético temprano y tectónica sedimentaria. *Acta Geol. Hisp.*, **37,** 355–368.

**Butler, G.P., Harris, P.M.** and **Kendall, C.G.S.C.** (1982) Recent evaporites from Abu Dhabi coastal flats. In: *Depositional and Diagenetic Spectra of Evaporites – A Core Workshop* (Eds C.R. Handford, R.G. Loucks and G.R. Davis), **3,** 33–64. Society of Economic Paleontologists and Mineralogists, Calgary.

**Casas, A.M.** (1992) El frente norte de las sierras de Cameros: estructuras cabalgantes y campo de esfuerzos. *Rev. Zubía*, **4,** 1–200. Ediciones Instituto Estudios Riojanos, Logroño (Spain).

**Coloma López, P., Sánchez Navarro, J.A., Martínez Gil, F.J.** and **Pérez, A.** (1997) El drenaje subterráneo de la Cordillera Ibérica en la Depresión terciaria del Ebro. *Rev. Soc. Geol. Esp.*, **10,** 205–218.

**Curtis, R., Evans, G., Kinsman, D.J.J.** and **Shearman, D.J.** (1963) Association of dolomite and anhydrite in the recent sediments of the Persian Gulf. *Nature*, **197,** 679–680.

**Evans, G., Schmidt, V., Bush, R.P.** and **Nelson, H.** (1969) Stratigraphy and geological history of the sabkha, Abu Dhabi, Persian Gulf. *Sedimentology*, **12,** 145–159.

**García Veigas, J.** (1997) First continental evaporitic phase in the South Pyrenean central area: Tremp Gypsum (Garumn facies, Upper Paleocene; Allochthonous Zone). In: *Sedimentary Deposition in Rift and Foreland Basins in France and Spain, Paleogene and Lower Neogene* (Eds G. Busson and B.Ch. Schreiber), pp. 335–342. Columbia University Press, New York.

**Guimerà, J.** and **Álvaro, M.** (1990) Structure et évolution de la compression alpine dans la Chaine Ibérique *et al.* Chaine cotière catalane (Espagne). *Bull. Soc. Géol. Fr.*, **6,** 339–348.

**Hanshaw, B.B.** and **Bredehoeft, J.D.** (1968) On the maintenance of anomalous fluid pressures; 2, source layer at depth. *Geol. Soc. Am. Bull.*, **79,** 1107–1122.

**Hardie, L.A.** (1967) The gypsum-anhydrite equilibrium at one atmosphere pressure. *Am. Mineral.*, **52,** 171–200.

**Hovorka, S.D.** (1992) Halite pseudomorphs after gypsum in bedded anhydrite: clue to gypsum-anhydrite relationships. *J. Sed. Petrol.*, **62,** 1098–1111.

**Jowett, E.C., Cathles, L.M., III** and **Davis, B.W.** (1993) Predicting depths of gypsum dehydration in evaporitic sedimentary basins. *AAPG Bull.*, **77,** 402–413.

**Kasprzyk, A.** (2003) Sedimentological and diagenetic patterns of anhydrite deposits in the Badenian evaporite basin of the Carpathian Foredeep, southern Poland. *Sed. Geol.*, **158,** 167–194.

**Kasprzyk, A.** and **Ortí, F.** (1998) Palaeogeographic and burial controls on anhydrite genesis: the Badenian basin in the Carpathian Foredeep (southern Poland, western Ukraine). *Sedimentology*, **45,** 889–907.

**Kinsman, D.J.J.** (1969) Modes of formation, sedimentary associations, and diagnostic features of shallow-water and supratidal evaporites. *AAPG Bull.*, **53,** 830–840.

**Kinsman, D.J.J.** (1976) Evaporites: relative humidity control of primary mineral facies. *J. Sed. Petrol.*, **46,** 273–279.

**Kuroda, H.** (1977) Mechanism of formation of the Furutobe Kuroko ore deposits – ore deposits and exploration at the Furutobe mine (II). *Min. Geol.*, **27,** 9–22. (in Japanese).

**Land, L.S.** (1995a) The role of saline formation water in crustal cycling. *Aquat. Geochem.*, **1,** 137–145.

**Land, L.S.** (1995b) Na-Ca-Cl saline formation waters, Frio Formation (Oligocene), south Texas, USA: products of diagenesis. *Geochim. Cosmochim. Acta*, **59,** 2163–2174.

**Lokier, S.W.** and **Steuber, T.** (2008) Quantification of carbonate ramp sedimentation and progradation rates for the Late Holocene Abu Dhabi shoreline. *J. Sed. Res.*, **78,** 423–431.

**Longinelli, A.** and **Craig, H.** (1967) Oxygen-18 variations in sulfate ions in sea-water and saline lakes. *Science*, **156,** 1431–1438.

**Lugli, S.** (1999) Geology of the Realmonte salt deposit, a desiccated Messinian Basin (Agrigento, Sicily). *Soc. Geol. Ital. Mem.*, **54,** 75–81.

**Lugli, S.** and **Testa, G.** (1993) The origin of the gypsum alabaster spheroids in the Messinian evaporites from Castellina Marittima (Pisa, Italy): preliminary observations. *Giorn. Geol.*, ser. 3ª, **55/1,** 51–68.

**Lugli, S., Schreiber, B.C.** and **Triberti, B.** (1999) Giant polygons in the Realmonte mine (Agrigento, Sicily): evidence for the desiccation of a Messinian halite basin. *J. Sed. Res.*, **69,** 764–771.

**MacDonald, G.J.F.** (1953) Anhydrite-gypsum equilibrium relations. *Am. J. Science*, **251,** 884–898.

**Marchal, C.** (1983) Le gîte salifère keupérien de Lorraine – Champagne et les formations asocies. Etude géometrique. Implications génétiques. *Mém. Sci. Terre*, **44,** 1–139. Fondation Scientifique de la Géologie et de ses applications, Nancy.

**Marshall, W.L.** and **Slusher, R.** (1966) Thermodynamics of calcium sulfate dihydrate in aqueous sodium chloride solutions, 0–110º. *J. Phys. Chem.*, **70,** 4015–4028.

**Martínez-Gil, F.J., Sánchez, J.A.** and **De Miguel, J.L.** (1988) El drenaje subterráneo de la Cordillera Ibérica en la Cuenca del Ebro con procesos de movilización y transporte de

substancias en disolución, sus implicaciones en el aporte de sulfatos. In: *Sistemas lacustres neógenos del Margen Ibérico de la Cuenca del Ebro* (Eds A. Pérez, A. Muñoz and A. Sánchez), pp. 57–80. Publicaciones de la Universidad de Zaragoza, Zaragoza.

**Moine, B., Sauvan, P.** and **Jarousse, J.** (1981) Geochemistry of evaporite-bearing series: a tentative guide for identification of metaevaporites. *Contrib. Mineral. Petrol.*, **76,** 401–412.

**Moldovanyi, E.P.** and **Walter, L.M.** (1992) Regional trends in water chemistry, Smackover Formation, southwest Arkansas: geochemical and physical controls. *AAPG Bull.*, **76,** 864–894.

**Muñoz-Jiménez, A.** (1992) *Análisis tectosedimentario del Terciario del sector occidental de la Cuenca del Ebro (Comunidad de La Rioja)*. Ciencias de la Tierra, 15. Ediciones del Instituto de estudios Riojanos, Logroño (España), 347 p.

**Murray, R.C.** (1964) Origin and diagenesis of gypsum and anhydrite. *J. Sed. Petrol.*, **34,** 512–523.

**Ortí, F.** (1989) Evaporites in Spain: marine vs. continental deposition. *28th International Geological Congress*, Washington, Abstracts Vol. **2,** 553–554.

**Ortí, F.** (1997) Evaporite sedimentation in the South Pyrenean Foredeeps and the Ebro Basin during the Tertiary: a general view. In: *Sedimentary Deposition in Rift and Foreland Basins in France and Spain, Paleogene and Lower Neogene* (Eds G. Busson and B.Ch. Schreiber), pp. 319–334. Columbia University Press, New York.

**Ortí, F.** and **Rosell, L.** (2000) Evaporative systems and diagenetic patterns in the Calatayud Basin (Miocene, central Spain). *Sedimentology*, **47,** 665–685.

**Ortí, F.** and **Rosell, L.** (2007) The Ninyerola Gypsum unit: an example of cyclic, lacustrine sedimentation (Middle Miocene, E Spain). *J. Iberian Geol.*, **33,** 249–260.

**Ortí, F.** and **Salvany, J.M.** (1997) Continental evaporitic sedimentation in the Ebro Basin during Miocene. In: *Sedimentary Deposition in Rift and Foreland Basins in France and Spain, Paleogene and Lower Neogene* (Eds G. Busson and B.Ch. Schreiber), pp. 420–429. Columbia University Press, New York.

**Ortí, F.** and **Salvany, J.M.** (2004) Coastal salina evaporites of the Triassic-Liassic boundary in the Iberian Peninsula: the Alacón borehole. *Geol. Acta*, **2,** 291–304.

**Ortí, F., Salvany, J.M., Rosell, L.** and **Inglès, M.** (1989a) Sistemas lacustres evaporíticos del Terciario de la Cuenca del Ebro. *Geogaceta*, **6,** 103–104. Sociedad Geológica de España, Madrid.

**Ortí, F., Rosell, L., Salvany, J.M., Inglès, M., Permanyer, A.** and **García-Veigas, J.** (1989b) Sedimentología y diagénesis como criterios de prospección en el Terciario evaporítico de la Cuenca del Ebro. XII Congreso Español Sedimentología, Bilbao. *Simposios*, **II,** 253–262.

**Ortí, F., Rosell, L.** and **Anadón, P.** (2003) Deep to shallow lacustrine evaporites in the Libros Gypsum (southern Teruel Basin, Miocene, NE Spain): an occurrence of pelletal gypsum rhythmites. *Sedimentology*, **50,** 361–386.

**Ortí, F., Rosell, L., Inglès, M.** and **Playà, E.** (2007) Depositional models of lacustrine evaporites in the SE margin of the Ebro Basin (Paleogene, NE Spain). *Geol. Acta*, **5,** 19–34.

**Ortí, F., Rosell, L., Playà, E.** and **García-Veigas, J.** (2010) Large gypsum nodules in the Paleogene-Neogene evaporites of Spain: distribution and significance. *Geol. Q.*, **54,** 411–422. Polish Geological Institute, Warszawa.

**Osborn, W.L.** (1989) *Formation, diagenesis and metamorphism of sulfate minerals in the Salton Sea geothermal system, California, U.S.A.* Master Thesis, University of California, Riverside, CA.

**Pierre, C.** (1982) *Teneurs en isotopes stables (18O, 2H, 13C, 34S) et conditions de genèse des evaporates marines. Applications à quelques milieux actuels et au Messinien de la Mediterranée*. Doctoral Thesis, Université Paris-Sud (Orsay), 266pp.

**Pierre, C.** (1985) Isotopic evidence for the dynamic redox cycle of dissolved sulphur compounds between free and interstitial solutions in marine salt pans. *Chem. Geol.*, **53,** 191–196.

**Robinson, B.E.** and **Kusakabe, M.** (1975) Quantitative preparation of sulfur dioxide, for $^{34}S/^{32}S$ analysis, from sulfides by combustion with cuprous oxide. *Anal. Chem.*, **47,** 1179–1181.

**Rodríguez-Aranda, J.P.** and **Calvo, J.P.** (1998) Trace fossils and rhizoliths as a tool for sedimentological and palaeoenvironmental analysis of ancient continental evaporite successions. *Palaeogeogr. Palaeoclimatol. Palaeoecol.*, **140,** 383–399.

**Salvany, J.M.** and **Ortí, F.** (1994) Miocene glauberite deposits of Alcanadre, Ebro Basin, Spain: sedimentary and diagenetic processes. In: *Sedimentology and Geochemistry of Modern and Ancient Saline Lakes* (Eds R.W. Renault and W.M. Last), *SEPM Spec. Publ.*, **50,** 203–215.

**Salvany, J.M., Muñoz, A.** and **Pérez, A.** (1994) Nonmarine evaporitic sedimentation and associated diagenetic processes of the southwestern margin of the Ebro Basin (Lower Miocene), Spain. *J. Sed. Res.*, **A64,** 190–203.

**Salvany, J.M., García-Veigas, J.** and **Ortí, F.** (2007) Glauberite-halite association of the Zaragoza Gypsum Formation (Lower Miocene, Ebro Basin, NE Spain). *Sedimentology*, **54,** 443–467.

**San Román, J., Sánchez, J.A.** and **Martínez Gil, F.J.** (1989) El drenaje subterráneo del macizo del Moncayo: aspectos hidrológicos e hidroquímicos. *Turiaso IX*, v. **1,** Revista del Centro de Estudios Turiasonenses, CSIC-Tarazona de Aragón (Zaragoza), 203–224.

**Sánchez Navarro, J.A., Martínez Gil, J., De Miguel, J.L., Pérez, A.** and **Martínez Gil, F.J.** (1992) Isopiezas y direcciones de flujo en el acuífero carbonatado mesozoico del margen ibérico de la Depresión del Ebro. *Geogaceta*, **11,** 122–124.

**Sánchez Navarro, J.A., Coloma López, P.** and **Pérez-García, A.** (2004) Evaluation of geothermal flow at the springs in Aragón (Spain) and its relation to geologic structure. *Hydrogeol. J.*, **12,** 601–609.

**Sánchez, J.A., Coloma, P.** and **Pérez, A.** (1999) Sedimentary processes related to the groundwater flows from the Mesozoic Carbonate Aquifer of the Iberian Chain in the Tertiary Ebro Basin, northeast Spain. *Sed. Geol.*, **129,** 201–213.

**Shearman, D.J.** (1966) Origin of marine evaporites by diagenesis. *Trans. Inst. Min. Metall.*, **75,** 207–215.

**Shearman, D.J.** (1985) Syndepositional and late diagenetic alteration of primary gypsum to anhydrite. In: *Sixth International Symposium on Salt 1983* (Eds B.C. Schreiber and H. Harner), Vol. **1,** pp. 41–50. The Salt Institute, Alexandria, VA.

**Shikazono, N., Holland, H.D.** and **Quirk, R.** (1983) Anhydrite in Kuroko deposits: mode of occurrence and depositional mechanisms. *Econ. Geol. Monogr.*, **5,** 329–344.

**Strohmenger, Ch.J., Al-Mansoori, A., Al-Jeelani, O., Al-Shamry, A., Al-Hosani, I., Al-Mehsin, K.** and **Shebl, H.** (2010) The sabkha sequence at Mussafah Channel (Abu Dhabi, United Arab Emirates): Facies stacking patterns,

microbial-mediated dolomite and evaporite overprint. *GeoArabia*, **15,** 49–90.

**Testa, G.** and **Lugli, S.** (2000) Gypsum-anhydrite transformations in Messinian evaporites of central Tuscany (Italy). *Sed. Geol.*, **130,** 249–268.

**Truc, G.** (1983) Dynamique de l'anhydritisation et du passage au gypse secondaire dans les évaporites paléogènes du bassin de Carpentras (Vaucluse, SE de la France). Documents du GRECO 52, no. 4: *Evaporites et milieux évaporitiques actuels et ancients*, Paris, 26–27 April 1983. Resumés de communications, Paris, 29 pp.

**Utrilla, R., Ortí, F., Pierre, C.** and **Pueyo, J.J.** (1991) Composición isotópica de las evaporitas terciarias continentales de la Cuenca del Ebro: relación con los ambientes deposicionales. *Rev. Soc. Geol. Esp.*, **4,** 353–360.

**Utrilla, R., Pierre, C., Ortí, F.** and **Pueyo, J.J.** (1992) Oxygen and sulphur isotope compositions as indicators of the origin of Mesozoic and Cenozoic evaporites from Spain. *Chem. Geol.*, **102,** 229–244.

**Warren, J.K.** (1991) Sulfate dominated sea-marginal and platform evaporative settings. In: *Evaporites, Petroleum and Mineral Resources* (Ed. J.L. Melvin), *Dev. Sedimentol.*, **50,** 477–533. Amsterdam, Elsevier.

**Warren, J.K.** (2006) *Evaporites: Sediments, Resources and Hydrocarbons*. Springer, Berlin, 1035 pp.

**Wood, W.W., Sandford, W.E.** and **Al-Habashi, A.R.** (2002) Source of solutes to the coastal sabkha of Abu Dhabi. *Geol. Soc. Am. Bull.*, **114,** 259–268.

**Worden, R.H., Smalley, P.C.** and **Fallick, A.E.** (1997) Sulfur cycle in buried evaporites. *Geology*, **25,** 643–646.

*Manuscript received 4 March 2011; revision accepted 19 October 2011*